

## Ⅱ 研究成果の刊行に関する一覧

研究成果の刊行に関する一覧表

雑誌

著者名	論文タイトル名	発表誌名	巻名	ページ	出版年
Komura D, H Nakamura, S Tsutsumi, H Aburatani and S Ihara	Multidimensional Support Vector Machines for visualization of gene expression data	Bioinformatics			in press
Houjun Liu, Yoichi Moroi, Shinichiro Yasumoto, Hisashi Kokuba, Shinichi Imafuku, Tetsuya Koga, Teiichi Masuda, Yating Tu, Masutaka Furue, Kazunori Urabe	Immunohistochemical localization of activated Stat3 and hTERT protein in psoriasis vulgaris	Br J Dermatol			in press
Ge X, Yamamoto S, Tsutsumi S, Midorikawa Y, Ihara S, Wang SM, Aburatani H.	Interpreting expression profiles of cancers by genome-wide survey of breadth-of-expression in normal tissues	Genomics			in press
Kano M, Tsutsumi S, Kawahara N, Wang Y, Mukasa A, Kirino T, Aburatani H	A meta-clustering analysis indicates distinct pattern alteration between two series of Gene Expression profiles for induced ischemic tolerance in rats	Physiological Genomics			in press
Kurahashi H, Taniguchi M, Meno C, Taniguchi Y, Takeda S, Horie M, Otani H, Toda T	Basement membrane fragility underlies embryonic lethality in fukutin-null mice	Neurobiol Dis			in press
Komura D, Nakamura H, Tsutsumi S, Aburatani H, Ihara S	Multidimensional support vector machines for visualization of gene expression data	Bioinformatics	21(4)	439-44	2005
Harada, M, Qin, Y, Takano, H, Minamino, T, Zou, Y, Toko, H, Ohtsuka, M, Matsuura, K, Sano, M, Nishi, J, Akazawa, H, Kunieda, T, Zhu, W, Hasegawa, H, Kunisada, K, Nagai, T, Nakaya, H, Yamauchi-Takahara, K, Komuro, I	G-CSF prevents cardiac Remodeling after myocardial infarction by activating Jak/Stat in cardiomyocytes	Nat Med	11	305-311	2005
Morita K, Urabe K, Moroi Y, Koga T, Nagai R, Horiuchi S, Furue M	Migration of keratinocytes is impaired on glycosylated collagen I	Wound Repair Regen	13	93-101	2005
Kobayashi J, Inai T, Morita K, Moroi Y, Urabe K, Shibata Y, Furue M	Reciprocal regulation of permeability through a cultured keratinocyte sheet by IFN-gamma and IL-4	Cytokine	7	186-9	2005
Midorikawa Y, Tsutsumi S, Nishimura K, Kamimura N, Kano M, Sakamoto H, Makuuchi M, Aburatani H	Distinct chromosomal bias of gene expression signatures in the progression of hepatocellular carcinoma	Cancer Res	64(20)	7263-70	2004
Minami T, Horiuchi K, Miura M, Abid R, Takabe W, Kohro T, Ge X, Aburatani H, Hamakubo T, Kodama T, Aird WC	VEGF- and thrombin-induced termination factor, down syndrome critical region-1, attenuates endothelial cell proliferation, and angiogenesis	J Biol Chem	279(48)	50537-54	2004
Kamei Y, Miura S, Suzuki M, Kai Y, Mizukami J, Taniguchi T, Mochida K, Hata T, Matsuda J, Aburatani H, Nishino I, Ezaki O	Skeletal muscle FOXO1 (FKHR)-transgenic mice have less skeletal muscle mass, down-regulated type I (slow twitch / red muscle) fiber genes, and impaired glycemic control	J Biol Chem	279(39)	41114-23	2004
Watanabe T, Akishita M, Nakaoka T, He H, Miyahara Y, Yamashita N, Wada Y, Aburatani H, Yoshizumi M, Kozaki K, Ouchi Y	Caveolin-1, Id3a and two LIM protein genes are upregulated by estrogen in vascular smooth muscle cells	Life Sci	75(10)	1219-29	2004
Kohro T, Tanaka T, Murakami T, Wada Y, Aburatani H, Hamakubo T, Kodama T	A Comparison of Differences in the Gene Expression Profiles of Phorbol 12-myristate 13-acetate Differentiated THP-1 Cells and Human Monocyte-derived Macrophage	J Atheroscler Thromb	11(2)	88-97	2004
Ogihara T, Asano T, Katagiri H, Sakoda H, Anai M, Shojima N, Ono H, Fujishiro M, Kushiya A, Fukushima Y, Kikuchi M, Noguchi N, Aburatani H, Gotoh Y, Komuro I, Fujita T	Oxidative stress induces insulin resistance by activating the nuclear factor-kappaB pathway and disrupting normal subcellular distribution of phosphatidylinositol 3-kinase	Diabetologia	47(5)	794-805	2004
Takita J, Ishii M, Tsutsumi S, Tanaka Y, Kato K, Toyoda Y, Hanada R, Yamamoto K, Hayashi Y, Aburatani H	Gene expression profiling and identification of novel prognostic marker genes in neuroblastoma	Genes Chromosomes Cancer	40(2)	120-32	2004
Hippo Y, Watanabe K, Watanabe A, Midorikawa Y, Yamamoto S, Ihara S, Tokita S, Iwanari H, Ito Y, Nakano K, Nezu J, Tsunoda H, Yoshino T, Ohizumi I, Tsuchiya M, Ohnishi S, Makuuchi M, Hamakubo T, Kodama T, Aburatani H	Identification of Soluble Amino Terminal Fragment of Glypican-3 as a Serological Marker for Early Stage Hepatocellular Carcinoma	Cancer Research	64(7)	2418-2423	2004
Mukasa A, Ueki K, Ge X, Ishikawa S, Ide T, Fujimaki T, Nishikawa R, Asai A, Kirino T, Aburatani H	Selective expression of a subset of neuronal genes in oligodendroglioma with chromosome 1p loss	Brain Pathology	14(1)	34-42	2004

Kawahara N, Wang Y, Mukasa A, Furuya K, Shimizu T, Hamakubo T, Aburatani H, Kodama T, Kirino T	Genome-wide Gene Expression Analysis for Induced Ischemic Tolerance and Delayed Neuronal Death Following Transient Global Ischemia in Rats	J Cereb Blood Flow Metab	24(2)	212-223	2004
Komura D, H Nakamura, S Tsutsumi, H Aburatani and S Ihara,	Incorporating prior Knowledge into clustering of gene expression profiles	International Conference on Genome Informatics	15	P036 1-2	2004
堤修一、井原茂男、油谷浩幸	アレイ技術とがん研究	血液、腫瘍科	48	182-189	2004
D Komura, H Nakamura, S Tsutsumi, H Aburatani and S Ihara,	Features of Gene Extraction by Nonlinear Support Vector Machines in Gene Expression Analysis	International Conference on Genome Informatics	14	322-323	2004
Minamino, T, Miyauchi, H, Yoshida, T, Tateno, K, Komuro, I	The role of vascular cell senescence in atherosclerosis: antisenesence as a novel therapeutic strategy for vascular aging	Curr Vasc Pharmacol	2	141-148	2004
Ohtsuka, M, Takano, H, Suzuki, M, Zou, Y, Akazawa, H, Tamagawa, M, Wakimoto, K, Nakaya, H, Komuro, I	Role of Na <sup>+</sup> -Ca <sup>2+</sup> exchanger in myocardial ischemia/reperfusion injury: evaluation using a heterozygous Na <sup>+</sup> -Ca <sup>2+</sup> exchanger knockout mouse model	Biochem Biophys Res Commun	314	849-853	2004
Longman C, Mercuri E, Cowan F, Allsop J, Brockington M, Jimenez-Mallebrera C, Kumar S, Rutherford M, Toda T, Muntoni F	Antenatal and postnatal brain magnetic resonance imaging in muscle-eye-brain disease	Arch Neurol	61	1301-1306	2004
Kurahashi H, Inagaki H, Yamada K, Ohye T, Taniguchi M, Emanuel BS, Toda T	Cruciform DNA structure underlies the etiology for palindrome-mediated human chromosomal translocations	J Biol Chem	279	35377-35383	2004
Moroi Y, Yu B, Urabe K, Koga T, Nakahara T, Dainichi T, Uchi H, Furue M	Effects of MAPK inhibitors on CCR4-mediated chemotaxis against thymus and activation-regulated chemokine (TARC/CCL17)	J Dermatol Sci	36	186-8	2004
Nakahara T, Uchi H, Urabe K, Chen Q, Furue M, Moroi Y	Role of c-Jun N-terminal kinase on lipopolysaccharide induced maturation of human monocyte-derived dendritic cells	Int Immunol	16	1701-9	2004
Masuda T, Furue M, Matsuda T	Photocured, styrenated gelatin-based microspheres for de novo adipogenesis through corelease of basic fibroblast growth factor, insulin, and insulin-like growth factor I	Tissue Eng	10	523-35	2004
Fujii-Maeda S, Kajiwara K, Ikizawa K, Shinazawa M, Yu B, Koga T, Furue M, Yanagihara Y	Reciprocal regulation of thymus and activation-regulated chemokine/macrophage-derived chemokine production by interleukin (IL)-4/IL-13 and interferon-gamma in HaCaT keratinocytes is mediated by alterations in E-cadherin distribution	J Invest Dermatol	122	20-28	2004
Minami, T, Murakami, T, Horiuchi, K, Miura, M, Noguchi, T, Miyazaki, JI, Hamakubo, T, Aird, WC, and Kodama, T	Interaction between Hex and GATA transcription factors in vascular endothelial cells inhibits flk-1/KDR-mediated VEGF signaling	J Biol Chem	279	20626-20635	2004
Minami, T, Sugiyama, A, Wu, SQ, Abid, R, Kodama, T, and Aird, WC	Thrombin and Phenotype Modulation of the Endothelium	Arterioscler Thromb Vasc Biol	24	41-53	2004
Abid MR, Guo S, Minami T, Spokes KC, Ueki K, Skurk C, Walsh K, and Aird WC		Arterioscler Thromb Vasc Biol	24	294-300	2004
Ge X, Tsutsumi S, Aburatani H, Iwata S	Reducing false positives in molecular pattern recognition	Genome Informatics	14	34-43	2003
Tsutsumi S, Taketani T, Nishimura K, Ge X, Taki T, Sugita K, Ishii E, Hanada R, Ohki M, Hayashi Y and Aburatani H	Two distinct gene expression signatures in pediatric acute lymphoblastic leukemia with MLL rearrangements	Cancer Research	63(16)	4882-4887	2003
Kano M, Nishimura K, Ishikawa S, Tsutsumi S, Hirota K, Hirose M, Aburatani H	Expression Imbalance Map: A New Visualization Method for Detection of mRNA Expression Imbalance Regions	Physiol Genomics	13	31-46	2003
井原茂男、堤修一、油谷浩幸		ゲノム医学	vol 3 No2	205-213	2003
Akazawa, H, Komuro, I	Roles of cardiac transcription factors in cardiac hypertrophy	Circ Res	92	1079-1088	2003
Hasegawa, H, Yamamoto, R, Takano, H, Mizukami, M, Asakawa, M, Nagai, T, Komuro, I	3-Hydroxy-3-methylglutaryl coenzyme A reductase inhibitors prevent the development of cardiac hypertrophy and heart failure in rats	J Mol Cell Cardiol	35	953-960	2003
Zou, Y, Zhu, W, Sakamoto, M, Qin, Y, Akazawa, H, Toko, H, Mizukami, M, Takeda, N, Minamino, T, Takano, H, Nagai, T, Nakai, A, Komuro, I	Heat shock transcription factor 1 protects cardiomyocytes from ischemia/reperfusion injury	Circulation	108	3024-3030	2003
Noguchi S, Tsukahara T, Fujita M, Kurokawa R, Tachikawa M, Toda T, Tsujimoto A, Arahata K, Nishino I	cDNA microarray analysis of individual Duchenne muscular dystrophy patients	Hum Mol Genet	12	595-600	2003

Takeda S, Kondo M, Sasaki J, Kurahashi H, Kano H, Arai K, Misaki K, Fukui T, Kobayashi K, Tachikawa M, Imamura M, Nakamura Y, Shimizu T, Murakami T, Sunada Y, Fujikado T, Matsumura K, Terashima T, Toda T	Fukutin is required for maintenance of muscle integrity, cortical histiogenesis and normal eye development	Hum Mol Genet	12	1449-1459	2003
Manya H, Sakai K, Kobayashi K, Taniguchi K, Kawakita M, Toda T, Endo E	Loss-of-function of an N-acetylglucosaminyltransferase, POMGnT1, in muscle-eye-brain disease	Biochem Biophys Res Commun	306	93-97	2003
Zhang W, Vajsar J, Cao P, Breningstall G, Diesen C, Dobyns W, Herrmann R, Lehesjoki A-E, Steinbrecher A, Talim B, Toda T, Topaloglu H, Voit T, Schachter H	Enzymatic diagnostic test for muscle-eye-brain type congenital muscular dystrophy using commercially available reagents	Clin Biochem	36	339-344	2003
Toda T, Kobayashi K, Takeda S, Sasaki J, Kurahashi H, Kano H, Tachikawa M, Wang F, Nagai Y, Taniguchi K, Taniguchi M, Sunada Y, Terashima T, Endo T, Matsumura K	Fukuyama-type congenital muscular dystrophy (FCMD) and $\alpha$ -dystroglycanopathy	Congenit Anom	43	97-104	2003
Endo T, Toda T	Glycosylation in congenital muscular dystrophies	Biol Pharm Bull	26	1641-1647	2003
Taniguchi K, Kobayashi K, Saito K, Yamanouchi H, Ohnuma A, Hayashi YK, Manya H, Jin DK, Lee M, Parano E, Falsaperla R, Pavone P, van Coster R, Talim B, Steinbrecher A, Straub V, Nishino I, Topaloglu H, Voit T, Endo T, Toda T	Worldwide distribution and broader clinical spectrum of muscle-eye-brain disease	Hum Mol Genet	12	527-534	2003
Silan F, Yoshioka M, Kobayashi K, Simsek E, Tunc M, Alper M, Cam M, Guven A, Fukuda Y, Kinoshita M, Kocabay K, Toda T	A new mutation of the fukutin gene in a non-Japanese patient	Ann Neurol	53	392-396	2003
Uchi H, Koga T, Urabe K, Moroi Y, Furue M	CX-659S, a diaminoacil derivative, indirectly inhibits the function of Langerhans cells by blocking the MEK1/2-Erk1/2 pathway in keratinocytes	J Invest Dermatol	120	983-989	2003
Koga T, Duan H, Urabe K, Furue M	IFN- $\gamma$ -positive immunostaining in psoriatic lesional keratinocytes-reply to the comments of McKenzie and colleagues	Eur J Dermatol	13	99	2003
Minami T, Sugiyama A, Wu SQ, Abid R, Kodama T, and Aird WC		Arterioscler Thromb Vasc Biol	24	41-53	2003
Minamoto T, Komuro I, et al	Peripheral-blood or bone-marrow mononuclear cells for therapeutic angiogenesis?	Lancet	360	2083-2084	2002
Toko H Komuro, I, et al	Csx/Nkx2-5 is required for homeostasis and survival of cardiac myocytes in the adult Heart	J Biol Chem	277	24735-24743	2002
Yoshioka M, Kuroki S, Sasaki H, Baba K, Toda T	A variant of congenital muscular dystrophy	Brain Dev	24	24-29	2002
Kano H, Kobayashi K, Herrmann R, Tachikawa M, Manya H, Nishino I, Nonaka I, Straub V, Talim B, Voit T, Topaloglu H, Endo T, Yoshikawa H, Toda T	Deficiency of $\alpha$ -dystroglycan in muscle-eye-brain disease	Biochem Biophys Res Commun	291	1283-1286	2002
Zanoteli E, Rocha JC, Narumia LK, Fireman MA, Moura LS, Oliveira AS, Gabbai AA, Fukuda Y, Kinoshita M, Toda T	Fukuyama-type congenital muscular dystrophy: a case report in the Japanese population living in Brazil	Acta Neurol Scand	106	117-121	2002
Horie M, Kobayashi K, Takeda S, Nakamura Y, Lyons GE, Toda T	Isolation and characterization of the murine homologue of the Fukuyama-type congenital muscular dystrophy gene, fukutin	Genomics	80	482-486	2002
Kohda F, Koga T, Uchi H, Urabe K, Furue M	Histamine-induced IL-6 and IL-8 production are differentially modulated by IFN- $\gamma$ and IL-4 in human keratinocytes	J Dermatol Sci	28	34-41	2002
Chen Q, Koga T, Uchi H, Hara H, Terao H, Moroi Y, et al	Propionibacterium acnes-induced IL-8 production may be mediated by NF- $\kappa$ B activation in human monocytes	J Dermatol Sci	29	97-103	2002
Yu B, Koga T, Urabe K, Moroi Y, Maeda S, Yanagihara Y, et al	Differential regulation of thymus- and activation-regulated chemokine induced by IL-4, IL-13, TNF- $\alpha$ and IFN- $\gamma$ in human keratinocyte and fibroblast	J Dermatol Sci	30	29-36	2002

Wada, Y, Sugiyama, A, Yamamoto, T, Naito, M, Noguchi, N, Yokoyama, S, Tsujita, M, Kawabe, Y, Kobayashi, M, Izumi, A, Kohro, T, Tanaka, T, Niki, E, Hamakubo, T, and Kodama, T	Lipid accumulation in human coronary artery smooth muscle cells by LDL loading under hypoxic conditions	Arteriosclerosis, Thrombosis, and Vascular Biology	22(10)	1712-9	2002
---	---	--	--------	--------	------

### Ⅲ 研究成果の刊行物・別冊



## Multidimensional support vector machines for visualization of gene expression data

D. Komura<sup>1,\*</sup>, H. Nakamura<sup>1</sup>, S. Tsutsumi<sup>1</sup>, H. Aburatani<sup>2</sup>  
and S. Ihara<sup>1</sup>

<sup>1</sup>Research Center for Advanced Science and Technology and <sup>2</sup>Genome Science Division, Center for Collaborative Research, University of Tokyo, Tokyo 153-8904, Japan

Received on May 21, 2004; accepted on November 11, 2004  
Advance Access publication December 17, 2004

### ABSTRACT

**Motivation:** Since DNA microarray experiments provide us with huge amount of gene expression data, they should be analyzed with statistical methods to extract the meanings of experimental results. Some dimensionality reduction methods such as Principal Component Analysis (PCA) are used to roughly visualize the distribution of high dimensional gene expression data. However, in the case of binary classification of gene expression data, PCA does not utilize class information when choosing axes. Thus clearly separable data in the original space may not be so in the reduced space used in PCA. **Results:** For visualization and class prediction of gene expression data, we have developed a new SVM-based method called multidimensional SVMs, that generate multiple orthogonal axes. This method projects high dimensional data into lower dimensional space to exhibit properties of the data clearly and to visualize a distribution of the data roughly. Furthermore, the multiple axes can be used for class prediction. The basic properties of conventional SVMs are retained in our method: solutions of mathematical programming are sparse, and nonlinear classification is implemented implicitly through the use of kernel functions. The application of our method to the experimentally obtained gene expression datasets for patients' samples indicates that our algorithm is efficient and useful for visualization and class prediction.

**Contact:** komura@hal.rcast.u-tokyo.ac.jp

### 1 INTRODUCTION

DNA microarray has been the key technology in modern biology and helped us to decipher the biological system

because of its ability to monitor the expression levels of thousands of genes simultaneously. Since DNA microarray experiments provide us with huge amount of gene expression data, they should be analyzed with statistical methods to extract the meanings of experimental results.

A great number of supervised learning algorithms have been proposed and applied to classification of gene expression data (Golub *et al.*, 1999; Tibshirani *et al.*, 2002; Khan *et al.*, 2001). Support Vector Machines (SVMs) have been paid attention in recent years because of their good performance in various fields, especially in the area of bioinformatics including classification of gene expression data (Furey *et al.*, 2000). However, SVMs predict a class of test samples by projecting the data into one-dimensional space based on a decision function. As a result, information loss of the original data is enormous.

Some methods are used for projecting high dimensional data into lower dimensional space to clearly exhibit the properties of the data and to roughly visualize the distribution of the data. Principal Component Analysis (PCA) (Fukunaga, 1990) and its derivatives, e.g. Nonlinear PCA (Diamantaras and Kung, 1996) and Kernel PCA (Schölkopf *et al.*, 1998), are most widely used for this purpose (Huang *et al.*, 2003). One drawback of PCA analysis is, however, that class information is not utilized for class prediction because PCA chooses axes based on the variance of overall data. Thus clearly separable data in the original space may not be so in the reduced space used in PCA. Another method for visualization and reducing dimension of data is discriminant analysis. It chooses axes based on class information in terms of within- and between-class variance. However, it is reported that SVMs often outperform discriminant analysis (Brown *et al.*, 2000).

The main purpose of this paper is to cover the shortcoming of SVMs by introducing multiple orthogonal axes for reducing dimensions and visualization of gene expression data. To this end, we have developed multidimensional SVMs (MD-SVMs), a new SVM-based method that generates multiple orthogonal axes based on margin between two

\*To whom correspondence should be addressed.

Komura *et al.* (2004) Multidimensional Support Vector Machines for Visualization of Gene Expression Data. Symposium on Applied Computing, Proceedings of the 2004 ACM symposium on Applied computing, 175-179; <http://doi.acm.org/10.1145/967900.967936>

Copyright 2004 Association for Computing Machinery, Inc. Reprinted by permission. Direct permission requests to [permissions@acm.org](mailto:permissions@acm.org)

classes to minimize generalization errors. The axes generated by this method reduce dimensions of original data to extract information useful in estimating the discriminability of two classes. This method fulfills the requirement of both visualization and class prediction. The basic properties of SVMs are retained in our method: solutions of mathematical programming are sparse, and nonlinear classification of data is implemented implicitly through the use of kernel functions.

This paper is organized as follows. In Section 2, we introduce the fundamental of SVMs. In Section 3, we describe the algorithm of MD-SVMs. In Section 4 and 5, we show numerical experiments on real gene expression datasets and reveal that our algorithm is effective for data visualization and class prediction.

### 1.1 Notation

$\mathbb{R}$  is defined as the set of real numbers. Each component of a vector  $x \in \mathbb{R}^n$ ,  $i = 1, \dots, n$  will be denoted by  $x_i$ ,  $j = 1, \dots, n$ . The inner product of two vectors  $x \in \mathbb{R}^n$  and  $y \in \mathbb{R}^n$  will be denoted by  $x \cdot y$ . For a vector  $x \in \mathbb{R}^n$  and a scalar  $a \in \mathbb{R}$ ,  $a \leq x$  is defined as  $a \leq x_i$  for all  $i = 1, \dots, n$ . For an arbitrary variable  $x$ ,  $x^k$  is just a name of the variable with upper suffix, not defined as  $k$ -th power of  $x$ .

## 2 SUPPORT VECTOR MACHINES

Since details of SVMs are fully described in the articles (Vapnik, 1998; Cristianini and Shawe-Taylor, 2000), we briefly introduce the fundamental principle of SVMs in this section. We consider a binary classification problem, where a linear decision function is employed to separate two classes of data based on  $m$  training samples  $x_i \in \mathbb{R}^n$ ,  $i = 1, \dots, m$  with corresponding class values  $y_i \in \{\pm 1\}$ ,  $i = 1, \dots, m$ . SVMs map a data  $x \in \mathbb{R}^n$  into a higher, probably infinite, dimensional space  $\mathbb{R}^N$  than the original space with an appropriate nonlinear mapping  $\phi: \mathbb{R}^n \rightarrow \mathbb{R}^N$ ,  $n < N$ . They generate the linear decision function of the form  $f(x) = \text{sign}(w \cdot \phi(x) + b)$  in the high dimensional space, where  $w \in \mathbb{R}^N$  is a weight vector which defines a direction perpendicular to the hyperplane of the decision function, while  $b \in \mathbb{R}$  is a bias which moves the hyperplane parallel to itself. The optimal decision function given by SVMs is a solution of an optimization problem

$$\min_{w, \xi} \frac{1}{2} \|w\|^2 + C \sum_{i=1}^m \xi_i, \quad \text{s.t. } y_i(w \cdot \phi(x_i) + b) \geq 1 - \xi_i, \quad i = 1, \dots, m, \quad \xi \geq 0, \quad (1)$$

with  $C > 0$ . Here,  $\xi \in \mathbb{R}^m$  is a vector whose elements are slack variables and  $C \in \mathbb{R}$  is a regularization parameter for penalizing training errors. When  $C \rightarrow \infty$ , no training errors are allowed, and thus this is called hard margin classification. When  $0 < C < \infty$ , this is called soft margin

classification because it allows some training errors. Note that a geometric margin  $\gamma$  between two classes is defined as  $\frac{1}{\|w\|^2}$ . The optimization problem formalizes the tradeoff between maximizing margin and minimizing training errors. The problem is transformed into its corresponding dual problem by introducing lagrange multiplier  $\alpha \in \mathbb{R}^m$  and replacing  $\phi(x_i) \cdot \phi(x_j)$  by kernel function  $K(x_i, x_j) = \phi(x_i) \cdot \phi(x_j)$  to be solved in an elegant way of dealing with a high dimensional vector space. The dual problem is

$$\max_{\alpha} -\frac{1}{2} \sum_{i=1}^m \sum_{j=1}^m \alpha_i \alpha_j y_i y_j K(x_i, x_j) + \sum_{i=1}^m \alpha_i, \quad \text{s.t. } 0 \leq \alpha \leq C, \quad \sum_{i=1}^m \alpha_i y_i = 0. \quad (2)$$

By virtue of the kernel function, the value of the inner product  $\phi(x_i) \cdot \phi(x_j)$  can be obtained without explicit calculation of  $\phi(x_i)$  and  $\phi(x_j)$ . Finally, the decision function becomes  $f(x) = \text{sign}(\sum_{i=1}^m \alpha_i y_i K(x_i, x) + b)$ . by using kernel functions between training samples  $x_i$ ,  $i = 1, \dots, m$  and a test sample  $x$ .

## 3 MULTIDIMENSIONAL SUPPORT VECTOR MACHINES

In order to overcome the drawback that SVMs cannot generate more than one decision function, we propose a SVM-based method that can be used for both data visualization and class prediction in this section. We call this method multidimensional SVMs (MD-SVMs). We deal with the same problem as mentioned in Section 2. Conventional SVMs give an optimal solution set  $(w, b, \xi)$  which corresponds to a decision function, while our MD-SVMs give the multiple sets  $(w^k, b^k, \xi^k)$ ,  $k = 1, 2, \dots, l$  with  $l \leq n$ , so that all the directions  $w_k$  are orthogonal to one another. The orthogonal axes can be used for reducing the dimension of original data and data visualization in three dimensional space by means of projection. Here the first set  $(w^1, b^1, \xi^1)$  is equivalent to that obtained by conventional SVMs. Now we only refer to the steps of obtaining  $(w^k, b^k, \xi^k)$ ,  $k = 2, 3, \dots, l$ . In practice, the  $k$ -th set  $(w^k, b^k, \xi^k)$ ,  $k = 2, 3, \dots, l$  are found with iterative computations of the optimization problem

$$\min_{w^k, \xi^k} \frac{1}{2} \|w^k\|^2 + C \sum_{i=1}^m \xi_i^k, \quad \text{s.t. } y_i(w^k \cdot \phi(x_i) + b^k) \geq 1 - \xi_i^k, \quad i = 1, \dots, m, \quad \xi^k \geq 0, \quad w^k \cdot w^j = 0, \quad j = 1, \dots, k-1. \quad (3)$$

This problem differs from that of conventional SVMs in the last constraint  $w^k \cdot w^j = 0$ . The weight vector  $w^j$ ,  $j = 1, \dots, k-1$  should be computed in advance by solving



other optimization problems (3). The optimization problem is modified by introducing lagrange multipliers  $\alpha^k, \gamma^k \in \mathbb{R}^m$ ,  $\beta^k \in \mathbb{R}^{k-1}$  and kernel functions. The primal Lagrangian is

$$\begin{aligned} L(\mathbf{w}^k, b^k, \xi^k) &= \frac{1}{2} \|\mathbf{w}^k\|^2 + C \sum_{i=1}^m \xi_i^k \\ &+ \sum_{i=1}^m \alpha_i^k (1 - \xi_i^k - y_i(\mathbf{w}^k \cdot \phi(x_i) + b^k)) \\ &+ \sum_{j=1}^{k-1} \beta_j^k (\mathbf{w}^k \cdot \mathbf{w}^j) - \sum_{i=1}^m \gamma_i^k \xi_i. \end{aligned} \quad (4)$$

Consequently, the optimization problem is

$$\begin{aligned} \max_{\alpha^k, \beta^k} & -\frac{1}{2} \sum_{i=1}^m \sum_{j=1}^m \alpha_i^k \alpha_j^k y_i y_j K(x_i, x_j) \\ &+ \frac{1}{2} \sum_{i=1}^{k-1} \beta_i^k \beta_i^k (\mathbf{w}^i \cdot \mathbf{w}^i) + \sum_{i=1}^m \alpha_i^k, \\ \text{s.t. } & 0 \leq \alpha^k \leq C, \sum_{i=1}^m \alpha_i^k y_i = 0, \\ & \sum_{i=1}^m \alpha_i^k y_i (\phi(x_i) \cdot \mathbf{w}^j) = 0, j = 1, \dots, k-1 \end{aligned} \quad (5)$$

Here  $\phi(x_p) \cdot \mathbf{w}^q$  and  $\mathbf{w}^p \cdot \mathbf{w}^p$  are calculated recursively as follows:

$$\phi(x_p) \cdot \mathbf{w}^q = \sum_{i=1}^m \alpha_i^q y_i K(x_p, x_i) - \sum_{i=1}^{q-1} \beta_i^q (\phi(x_p) \cdot \mathbf{w}^i), \quad (6)$$

$$\begin{aligned} \mathbf{w}^p \cdot \mathbf{w}^p &= \sum_{i=1}^m \sum_{j=1}^m \alpha_i^p \alpha_j^p y_i y_j K(x_i, x_j) \\ &- \sum_{i=1}^m \sum_{j=1}^{p-1} \alpha_i^p y_i \beta_j^p (\phi(x_i) \cdot \mathbf{w}^j) + \sum_{i=1}^{p-1} \beta_i^p \beta_i^p (\mathbf{w}^i \cdot \mathbf{w}^i) \\ &- \sum_{i=1}^m \sum_{j=1}^{p-1} \alpha_i^p y_i \beta_j^p (\phi(x_i) \cdot \mathbf{w}^j), \end{aligned} \quad (7)$$

where  $\phi(x_p) \cdot \mathbf{w}^1 = \sum_{i=1}^m \alpha_i^1 y_i K(x_p, x_i)$  and  $\mathbf{w}^1 \cdot \mathbf{w}^1 = \sum_{i=1}^m \alpha_i^1 y_i (\phi(x_i) \cdot \mathbf{w}^1)$ . As can be seen, there is no need to calculate nonlinear map of data  $\phi(x)$  in problem (5) because all nonlinear mappings can be replaced with kernel functions.

Note that this optimization problem is a nonconvex quadratic problem when  $k$  is more than 1. As a consequence, the optimal solutions are not easy to be obtained. In Section 4, we use local optimum for numerical experiments when  $k$  is 2 or 3. We note the experimental results are still encouraging.

The corresponding Karush–Kuhn–Tucker conditions are

$$\alpha_i^k (1 - \xi_i^k - y_i(\mathbf{w}^k \cdot \phi(x_i) + b^k)) = 0, \quad (8)$$

$$\xi_i^k (\alpha_i^k - C) = 0, i = 1, \dots, m. \quad (9)$$

These are exactly the same as conventional SVMs. We highlight the other properties conserved from conventional SVMs:

- Projecting data into high dimensional space is implicit, using kernel functions to replace inner products.
- The solutions  $\alpha^k$  of the optimization problem is sparse. Then the corresponding decision function depends only on few ‘Support Vectors’.

Since each decision function is normalized independently to hold  $\mathbf{w}^k \cdot \phi(x_i) + b^k = y_i$  for  $i = 1, \dots, m$ , data scales of the axes should be aligned with first axis ( $k = 1$ ) for visualization. The margin  $\gamma^k$ , the L2-distance between support vectors of each class of  $k$ -th axis, is

$$\left( \sum_{i=1}^m \sum_{j=1}^m \alpha_i^k \alpha_j^k y_i y_j K(x_i, x_j) - \sum_{i=1}^{k-1} \beta_i^k \beta_i^k (\mathbf{w}^i \cdot \mathbf{w}^i) \right)^{-\frac{1}{2}}. \quad (10)$$

So a scaling factor  $s^k = \gamma^1 / \gamma^k$  is

$$\sqrt{\frac{\sum_{i=1}^m \sum_{j=1}^m \alpha_i^1 \alpha_j^1 y_i y_j K(x_i, x_j)}{\sum_{i=1}^m \sum_{j=1}^m \alpha_i^k \alpha_j^k y_i y_j K(x_i, x_j) - \sum_{i=1}^{k-1} \beta_i^k \beta_i^k (\mathbf{w}^i \cdot \mathbf{w}^i)}}. \quad (11)$$

The decision function of  $k$ -th step has the form  $f^k(x) = \text{sign}(\sum_{i=1}^m \alpha_i^k y_i K(x_i, x) + b^k)$ . Since the right hand side of the equation has the function of projecting original data into one dimensional space, the data can be plot in up to three dimensional space for visualization. The coordinate of data  $x \in \mathbb{R}^m$  in three dimensional space is

$$(s^{k1} g^{k1}(x), s^{k2} g^{k2}(x), s^{k3} g^{k3}(x)), \quad (12)$$

where  $g^k(x) = \sum_{i=1}^m \alpha_i^k y_i K(x_i, x) + b^k$ . The space represents a distribution of data clearly based on the margin between two classes.

## 4 NUMERICAL EXPERIMENTS

### 4.1 Method

In order to confirm the effectiveness of our algorithm, we have performed numerical experiments. MD-SVMs can generate multiple axes, up to the number of features. Here we choose three axes,  $k = 1, 2, 3$ , to simplify the experiments. When  $k$  is

2 or 3, we use local optimum in problem (5) since it is difficult to obtain the global solutions. In our experiments, we carry out hold-out validation because cross-validation changes decision functions every time the dataset is split. Then we compare the results obtained by MD-SVMs with those obtained by PCA.

In the experiments, the expression values for each of the genes are normalized such that the distribution over the samples has a zero mean and unit variance. Before normalization, we discard genes in the dataset with the overall average value less than 0.35. Then we calculate a score  $F(x(j)) = |(\mu^+(j) - \mu^-(j)) / (\sigma^+(j) + \sigma^-(j))|$ , for the remaining genes. Here  $\mu^+(j)$ ,  $\mu^-(j)$  and  $\sigma^+(j)$ ,  $\sigma^-(j)$  denote the mean and standard deviation of the  $j$ -th gene of the samples labeled +1(-1), respectively. This score becomes the highest when the corresponding expression levels of the gene differ most in the two classes and have small deviations in each class. We select 100 genes with the highest scores and use them for hold-out validation. These procedures for gene selection are done only for training data for fair experiments.

The regularization parameter  $C$  in problem (5) is set to 1000. This value is rather large but finite because we would like to avoid ill-posed problems in a hard margin classification. We choose linear kernel  $K(x_i, x_j) = x_i \cdot x_j$  and RBF kernel  $K(x_i, x_j) = \exp -\gamma \|x_i - x_j\|^2$  with  $\gamma = 0.001$  in the experiments of MD-SVMs.

## 4.2 Materials

**Leukemia dataset (Golub et al., 1999)** This gene expression dataset consists of 72 leukemia samples, including 25 acute myeloid leukemia (AML) samples and 47 acute lymphoblastic leukemia (ALL) samples. They are obtained by hybridization on the Affymetrix GeneChip containing probe sets for 7070 genes. Training set contains 20 AML samples and 42 ALL samples. Test set contains 5 AML samples and 5 ALL samples. AML samples are labeled +1 and ALL samples are labeled -1.

**Lung tissue dataset (Bhattacharjee et al., 2001)** This dataset consists of 203 samples from lung tissue, including 16 samples from normal tissue and 187 samples from cancerous tissue, and is obtained by hybridization on the Affymetrix U95A Genechip containing probe sets for 12558 genes. Training set includes 13 samples from normal tissue and 157 samples from cancerous tissue. Test set includes 3 samples from normal tissue and 30 samples from cancerous tissue. Samples from normal tissue are labeled +1 and samples from cancerous tissue are labeled -1.

## 5 RESULTS AND DISCUSSION

The results of numerical experiments are shown in Figure 1, and Tables 1 and 2. The distributions obtained by MD-SVMs on the leukemia dataset and the lung tissues dataset are given in Figure 1-(1) and 1-(3), respectively. Those obtained by PCA are given in Figure 1-(2) and 1-(4), respectively. The number

of misclassified samples by MD-SVMs are summarized in Table 1 and 2. In these tables, the class of the samples is predicted based on decision functions  $f^k(x)$ ,  $k = 1, 2, 3$ , corresponding to each of the three axes.

Figure 1-(1) and 1-(3) illustrate that MD-SVMs are likely to separate the samples of each class in all the three directions. However, as shown in Figure 1-(2) and 1-(4), PCA does not separate the samples in the directions of the 2nd or the 3rd axis. These axes by PCA are dispensable with the objective of visualization for class prediction. In other words, MD-SVMs gather the plots of the samples into the appropriate clusters of each class, while PCA rather scatters them. Furthermore, in the distribution by MD-SVMs for the lung tissues dataset, one sample outliers from correct clusters (indicated by arrows in Figure 1-(3)). Though this sample also seems to be an outlier in the distribution by PCA (also indicated in Figure 1-(4)), the outlier significantly deviates in MD-SVMs. This may arise from the fact that MD-SVMs can separate the samples in all the directions. These observations indicate that MD-SVMs are well suited for visualizing in binary classification problems.

The significant advantage of MD-SVMs over PCA is the ability to predict the classes. MD-SVMs can predict the classes of samples based on the decision functions  $f^k(x)$  without extra computation, while PCA cannot. The predicted class of a sample should be matched by the all the decision functions in an ideal case. However that does not always occur as seen in Tables 1 and 2. In such cases, the simplest method for prediction is to use only the 1st axis, which corresponds to the decision function generated by conventional SVMs. The idea is supported by the fact that the 1st decision function classifies the samples most correctly in almost all cases in Tables 1 and 2. The more advanced method is weighted voting. Scaling factor or normalized objective values in problem (5) are the candidate of the weight.

Multiple decision functions generated by MD-SVMs are useful for outlier detection. Samples misclassified by multiple decision functions may be mis-labeled or categorized into unknown classes. For example, see the column '3 axes' of test sample of the lung tissues dataset with RBF kernel in Table 2. This sample is misclassified by all decision functions, so we can say that this data contains some experimental error. The hierarchical clustering method also supports our result. These results indicate that MD-SVMs can be used for finding candidates of outliers.

## 6 CONCLUSION

For both visualization and class prediction of gene expression data, we propose a new method called Multidimensional Support Vector Machines. We formulate the method as a quadratic program and implement the algorithm. This is motivated by the following facts: (1) SVMs perform better than the other classification algorithms, but they generate only one axis for class prediction. (2) PCA chooses multiple

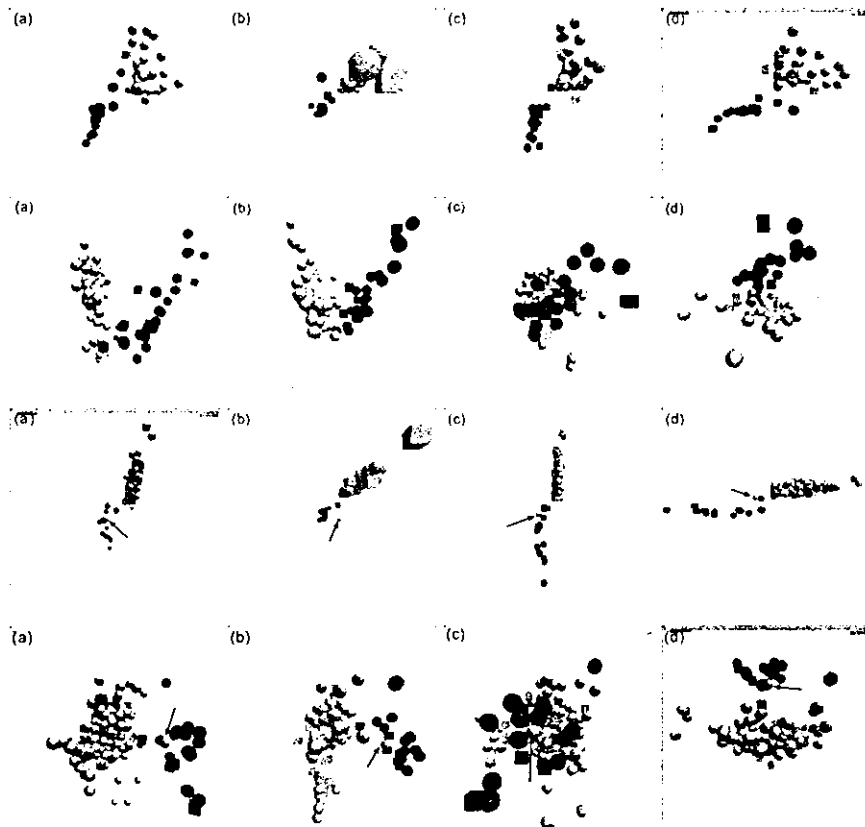


**Fig. 1.** (Top row) Distribution obtained by MD-SVMs for the leukemia dataset with linear kernel. (Second row) Distribution obtained by PCA on the leukemia dataset. (Third row) Distribution obtained by MD-SVMs for the lung tissues dataset with linear kernel. The sample indicated by arrows appears to be an outlier. (Fourth row) Distribution obtained by PCA for the lung tissues dataset. The sample indicated by arrows is the same as in the third row but with less deviates. (a) Cross shot, (b) 1st axis (x axis) and 2nd axis (y axis), (c) 2nd axis (x axis) and 3rd axis (y axis), (d) 3rd axis (x axis) and 1st axis (y axis). Black objects and white objects indicate AML samples (or normal tissues) ALL samples (or cancerous tissues), respectively. Training data and test data are expressed as a sphere and a cube, respectively.

**Table 1.** Number of classification errors in the MD-SVMs for the leukemia dataset. The columns ' $n$ -th axis',  $n = 1, 2, 3$ , indicates the number of samples misclassified by  $n$ -th decision function. The columns ' $n$  axes',  $n = 1, 2, 3$ , indicates the number of samples misclassified by  $n$  decision functions

Kernel	Sample	# of samples	1st axis	2nd axis	3rd axis	1 axis	2 axes	3 axes
Linear	Training	62	0	1	2	1	1	0
RBF	Training	62	0	2	7	5	2	0
Linear	Test	10	1	1	2	2	1	0
RBF	Test	10	0	2	0	2	0	0

**Table 2.** Number of classification errors in the MD-SVMs on the lung dataset. See the caption of Table 1 for other explanation

Kernel	Sample	# of samples	1st axis	2nd axis	3rd axis	1 axis	2 axes	3 axes
Linear	Training	170	0	1	1	0	1	0
RBF	Training	170	0	3	5	2	3	0
Linear	Test	33	1	0	0	1	0	0
RBF	Test	33	1	1	1	0	0	1

orthogonal axes, but it cannot predict classes of samples without other classification algorithms. We have tried to cover the shortcomings of both methods. MD-SVMs choose multiple orthogonal axes, which correspond to decision functions, from high dimensional space based on a margin between two classes. These multiple axes can be used for both visualization and class prediction.

Numerical experiments on real gene expression data indicate the effectiveness of MD-SVMs. All axes generated by MD-SVMs are taken into account for separating class of samples, while the 2nd and the 3rd axes by PCA are not. The samples in the distributions by MD-SVMs gather into appropriate clusters more vividly than those by PCA. MD-SVMs can predict the classes of the samples with multiple decision functions. We also indicate that MD-SVMs are useful for outlier detection with multiple decision functions.

There are several future works to be done on MD-SVMs: (1) application of our method to wider variety of gene expression datasets, (2) investigation of gene selection for preprocess of analysis and (3) investigation on class prediction method with multiple decision functions. Firstly, the use of more suitable samples may show that the axes chosen by MD-SVMs separate samples more clearly than those by PCA. Secondly, since the conventional SVMs show good generalization performance especially with large number of features, it is expected that MD-SVMs show much better performance than PCA with increasing the number of genes used in the numerical experiments. Since the element of weight vector generated by SVMs is one of the measures of discrimination power of the corresponding genes (Guyon *et al.*, 2002), that generated by MD-SVMs can be used for gene selection. Thirdly, the classification with probability as well as the weighted voting mentioned in Section 4 may be achieved in our scheme since the conventional SVMs have been already expanded for the purpose with sigmoid functions (Platt, 1999). We hope that our method sheds some lights on the future study of gene expression experiments.

## REFERENCES

- Bhattacharjee, A., Richards, W., Staunton, J., Li, C., Monti, S., Vasa, P., Ladd, C., Beheshti, J., Bueno, R., Gillette, M. *et al.* (2001) Classification of human lung carcinomas by mRNA expression profiling reveals distinct adenocarcinoma subclasses. *Proc. Natl Acad. Sci. USA*, **98**, 13790–13795.
- Brown, M., Grundy, W., Lin, D., Cristianini, N., Sugnet, C., Furey, T., Ares, M. and Haussler, D. (2000) Knowledge-based analysis of microarray gene expression data by using support vector machines. *Proc. Natl Acad. Sci. USA*, **97**, 262–267.
- Cristianini, N. and Shawe-Taylor, J. (2000) *An Introduction to Support Vector Machines and Other Kernel-based Learning Methods*. Cambridge University Press, NY.
- Diamantaras, K. and Kung, S. (1996) *Principal Component Neural Networks Theory and Applications*. John Wiley & Sons, NY.
- Fukunaga, K. (1990) *Introduction to Statistical Pattern Recognition*. Academic Press, NY.
- Furey, T., Cristianini, N., Duffy, N., Bednarski, D., Schummer, M. and Haussler, D. (2000) Support vector machine classification and validation of cancer tissue samples using microarray expression data. *Bioinformatics*, **16**, 906–914.
- Golub, T., Slonim, D., Tamayo, P., Huard, C., Gaasenbeek, M., Mesirov, J., Coller, H., Loh, M., Downing, J., Caligiuri, M., Bloomfield, C. and Lander, E. (1999) Molecular classification of cancer: class discovery and class prediction by gene expression monitoring. *Science*, **286**, 531–537.
- Guyon, I., Weston, J., Barnhill, S. and Vapnik, V. (2002) Gene selection for cancer classification using support vector machines. *J. Machine Learn.*, **46**, 389–422.
- Huang, E., Ishida, S., Pittman, J., Dressman, H., Bild, A., Kloos, M., D'Amico, M., Pestell, R., West, M. and Nevins, J. (2003) Gene expression phenotypic models that predict the activity of oncogenic pathways. *Nat. Genet.*, **34**, 226–230.
- Khan, J., Wei, J., Ringnér, M., Saal, L., Ladanyi, M., Westermann, F., Berthold, F., Schwab, M., Antonescu, C., Peterson, C. and Meltzer, P. (2001) Classification and diagnostic prediction of cancers using gene expression profiling and artificial neural networks. *Nat. Med.*, **7**, 673–679.
- Platt, J. (1999) *Probabilistic Outputs for Support Vector Machines and Comparisons to Regularized Likelihood Methods*. MIT Press, Cambridge, MA.
- Schölkopf, B., Smola, A. and Müller, K. (1998) Non-linear component analysis as a kernel eigenvalue problem. *Neural Comput.*, **10**, 1299–1319.
- Tibshirani, R., Hastie, T., Narasimhan, B. and Chu, G. (2002) Diagnosis of multiple cancer types by shrunken centroids of gene expression. *Proc. Natl Acad. Sci. USA*, **99**, 6567–6572.
- Vapnik, V. (1998) *Statistical Learning Theory*. John Wiley & Sons, NY.

# G-CSF prevents cardiac remodeling after myocardial infarction by activating the Jak-Stat pathway in cardiomyocytes

Mutsuo Harada<sup>1,4</sup>, Yingjie Qin<sup>1,4</sup>, Hiroyuki Takano<sup>1,4</sup>, Tohru Minamino<sup>1,4</sup>, Yunzeng Zou<sup>1</sup>, Haruhiro Toko<sup>1</sup>, Masashi Ohtsuka<sup>1</sup>, Katsuhisa Matsuura<sup>1</sup>, Masanori Sano<sup>1</sup>, Jun-ichiro Nishi<sup>1</sup>, Koji Iwanaga<sup>1</sup>, Hiroshi Akazawa<sup>1</sup>, Takeshige Kunieda<sup>1</sup>, Weidong Zhu<sup>1</sup>, Hiroshi Hasegawa<sup>1</sup>, Keita Kunisada<sup>2</sup>, Toshio Nagai<sup>1</sup>, Haruaki Nakaya<sup>3</sup>, Keiko Yamauchi-Takahara<sup>2</sup> & Issei Komuro<sup>1</sup>

Granulocyte colony-stimulating factor (G-CSF) was reported to induce myocardial regeneration by promoting mobilization of bone marrow stem cells to the injured heart after myocardial infarction, but the precise mechanisms of the beneficial effects of G-CSF are not fully understood. Here we show that G-CSF acts directly on cardiomyocytes and promotes their survival after myocardial infarction. G-CSF receptor was expressed on cardiomyocytes and G-CSF activated the Jak/Stat pathway in cardiomyocytes. The G-CSF treatment did not affect initial infarct size at 3 d but improved cardiac function as early as 1 week after myocardial infarction. Moreover, the beneficial effects of G-CSF on cardiac function were reduced by delayed start of the treatment. G-CSF induced antiapoptotic proteins and inhibited apoptotic death of cardiomyocytes in the infarcted hearts. G-CSF also reduced apoptosis of endothelial cells and increased vascularization in the infarcted hearts, further protecting against ischemic injury. All these effects of G-CSF on infarcted hearts were abolished by overexpression of a dominant-negative mutant Stat3 protein in cardiomyocytes. These results suggest that G-CSF promotes survival of cardiac myocytes and prevents left ventricular remodeling after myocardial infarction through the functional communication between cardiomyocytes and noncardiomyocytes.

Myocardial infarction is the most common cause of cardiac morbidity and mortality in many countries, and left ventricular remodeling after myocardial infarction is important because it causes progression to heart failure. Several cytokines including G-CSF, erythropoietin and leukemia inhibitory factor have beneficial effects on cardiac remodeling after myocardial infarction<sup>1–5</sup>. In particular, G-CSF markedly improves cardiac function and reduce mortality after myocardial infarction in mice, possibly by regeneration of myocardium and angiogenesis<sup>1,2,6–8</sup>. G-CSF is known to have various functions such as induction of proliferation, survival and differentiation of hematopoietic cells, as well as mobilization of bone marrow cells<sup>9–11</sup>. Although it was reported that bone marrow cells could differentiate into cardiomyocytes and vascular cells, thereby contributing to regeneration of myocardium and angiogenesis in ischemic hearts<sup>12–15</sup>, accumulating evidence has questioned these previous reports<sup>16–18</sup>. In this study, we examined the molecular mechanisms of how G-CSF prevents left ventricular remodeling after myocardial infarction.

## RESULTS

### G-CSF directly acts on cultured cardiomyocytes

G-CSF receptor (G-CSFR, encoded by *CSF3R*) has been reported to be expressed only on blood cells such as myeloid leukemic cells,

leukemic cell lines, mature neutrophils, platelets, monocytes and some lymphoid cell lines<sup>9</sup>. To test whether G-CSFR is expressed on mouse cardiomyocytes, we performed a reverse transcription–polymerase chain reaction (RT-PCR) experiment by using specific primers for mouse *Csf3r*. We detected expression of the *Csf3r* gene in the adult mouse heart and cultured neonatal cardiomyocytes (Fig. 1a). We next examined expression of G-CSFR protein in cultured cardiomyocytes of neonatal rats by immunocytochemistry. Similar to the previously reported expression pattern of G-CSFR in living cells<sup>19</sup>, the immunoreactivity for G-CSFR was localized to the cytoplasm and cell membrane under steady-state conditions in cardiomyocytes (Fig. 1b). This immunoreactivity disappeared when the antibody specific for G-CSFR was omitted, validating its specificity (Fig. 1b). In addition to cardiomyocytes, we also detected expression of G-CSFR on cardiac fibroblasts by immunocytochemistry (see Supplementary Fig. 1 online) and RT-PCR (Supplementary Fig. 2 online).

The binding of G-CSF to its receptor has been reported to evoke signal transduction by activating the receptor-associated Janus family tyrosine kinases (JAK) and signal transducer and activator of transcription (STAT) proteins in hematopoietic cells<sup>9,10</sup>. In particular, STAT3

<sup>1</sup>Department of Cardiovascular Science and Medicine, Chiba University Graduate School of Medicine, 1-8-1 Inohana, Chuo-ku, Chiba 260-8670, Japan. <sup>2</sup>Department of Molecular Medicine, Osaka University Medical School, Osaka University, 2-2 Yamadaoka, Suita, Osaka 565-0871, Japan. <sup>3</sup>Department of Pharmacology, Chiba University Graduate School of Medicine, 1-8-1 Inohana, Chuo-ku, Chiba 260-8670, Japan. <sup>4</sup>These authors contributed equally to this work. Correspondence should be addressed to I.K. (komuro-tky@umin.ac.jp).

Published online 20 February 2005; doi:10.1038/nm1199

ARTICLES

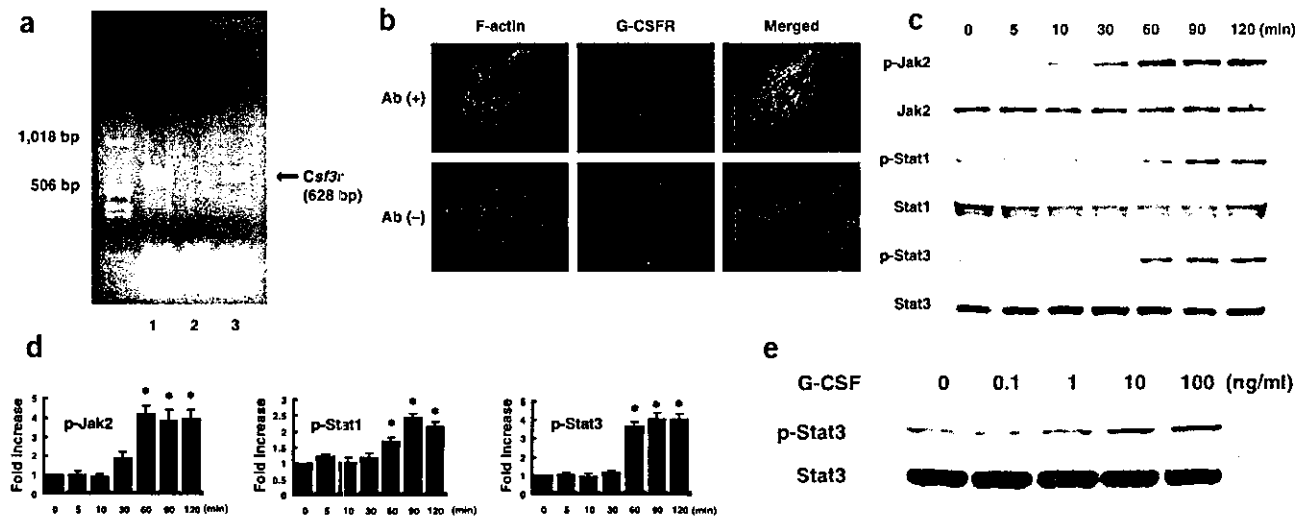


**Figure 1** Expression of G-CSFR and the G-CSF-evoked signal transduction in cultured cardiomyocytes. (a) RT-PCR for mouse *Csf3r*. Expression of *Csf3r* was detected in the adult mouse heart (lane 1) and cultured cardiomyocytes of neonatal mice (lane 3). In lane 2, reverse transcription products were omitted to exclude the possibility of false-positive results from contamination. (b) Immunocytochemical staining for G-CSFR. Cardiomyocytes from neonatal rats were incubated with antibody to G-CSFR (red) and phalloidin (green) (upper panel). In the absence of antibody to G-CSFR, no signal was detected (lower panel). Original magnification,  $\times 1,000$ . (c) G-CSF induces phosphorylation of Jak2, Stat1 and Stat3 in a time-dependent manner in cultured cardiomyocytes. (d) Quantification of Jak2, Stat1 and Stat3 activation by G-CSF stimulation as compared with control (time = 0). \* $P < 0.05$  versus control ( $n = 3$ ). (e) G-CSF induces phosphorylation and activation of Stat3 in a dose-dependent manner in cultured cardiomyocytes.

has been reported to contribute to G-CSF-induced myeloid differentiation and survival<sup>20,21</sup>. We therefore examined whether G-CSF activates the Jak-Stat signaling pathway in cultured cardiomyocytes. G-CSF (100 ng/ml) significantly induced phosphorylation and activation of Jak2 and Stat3, and to a lesser extent, Stat1 but not Jak1, Tyk2 or Stat5 in a dose-dependent manner (Fig. 1c–e and data not shown), suggesting that G-CSFR on cardiomyocytes is functional.

We next examined whether G-CSF confers direct protective effects on cardiomyocytes as it prevents hematopoietic cells from apoptotic death<sup>21</sup>. We exposed cardiomyocytes to 0.1 mM H<sub>2</sub>O<sub>2</sub> in the absence or presence of G-CSF and examined cardiomyocyte apoptosis by staining with annexin V<sup>22,23</sup>. Pretreatment with G-CSF significantly reduced the number of H<sub>2</sub>O<sub>2</sub>-induced annexin V-positive cells compared with cells that were not given the G-CSF pretreatment

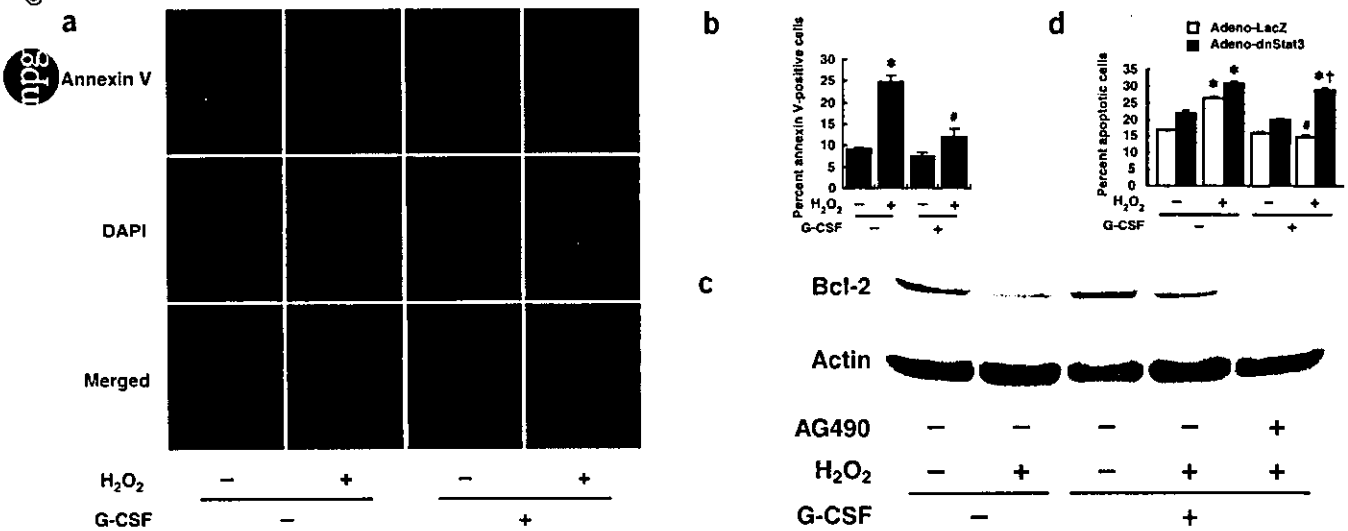


**Figure 2** Suppression of H<sub>2</sub>O<sub>2</sub>-induced cardiomyocyte apoptosis by G-CSF. (a) Detection of apoptosis by Cy3-labeled annexin V. Red fluorescence shows apoptotic cardiomyocytes stained with Cy3-labeled annexin V. Nuclei were counterstained with DAPI staining (blue). Original magnification,  $\times 400$ . (b) Quantitative analysis of apoptotic cells. The vertical axis indicates the ratio of the annexin V-positive cell number relative to that of DAPI-positive nuclei. \* $P < 0.01$  versus nontreated cells, # $P < 0.05$  versus H<sub>2</sub>O<sub>2</sub>-treated cells without G-CSF ( $n = 3$ ). (c) G-CSF prevents H<sub>2</sub>O<sub>2</sub>-induced downregulation of Bcl-2 expression ( $n = 3$ ). (d) Inhibition of antiapoptotic effects of G-CSF by Adeno-dnStat3. Bar graphs represent quantitative analysis of the apoptotic cell number relative to the total cell number. \* $P < 0.001$  versus H<sub>2</sub>O<sub>2</sub> (-)/G-CSF (-), # $P < 0.001$  versus H<sub>2</sub>O<sub>2</sub> (+)/G-CSF (-), † $P < 0.001$  versus H<sub>2</sub>O<sub>2</sub> (+)/G-CSF (+)/Adeno-LacZ ( $n = 3$ ).

(Fig. 2a,b). To investigate the molecular mechanism of how G-CSF exerts an antiapoptotic effect on cultured cardiomyocytes, we examined expression of the Bcl-2 protein family, known target molecules of the Jak-Stat pathway<sup>24</sup>, by western blot analysis. Expression levels of antiapoptotic proteins such as Bcl-2 and Bcl-xL were lower when cardiomyocytes were subjected to H<sub>2</sub>O<sub>2</sub> (Fig. 2c and data not shown), and this reduction was considerably inhibited by G-CSF pretreatment (Fig. 2c). AG490, an inhibitor of Jak2, abolished G-CSF-induced Bcl-2 expression (Fig. 2c) but did not affect its basal levels (Supplementary Fig. 3 online), suggesting a crucial role of the Jak-Stat pathway in inducing survival of cardiomyocytes by G-CSF. To further elucidate the involvement of the Jak-Stat pathway in the protective effects of G-CSF on cardiomyocytes, we transduced cultured cardiomyocytes with adenovirus encoding dominant-negative Stat3 (Adeno-dnStat3). G-CSF treatment significantly reduced apoptosis induced by H<sub>2</sub>O<sub>2</sub> in Adeno-LacZ-infected cardiomyocytes (Fig. 2d). This effect was abolished by introduction of Adeno-dnStat3 (Fig. 2d), suggesting that Stat3 mediates the protective effects of G-CSF on H<sub>2</sub>O<sub>2</sub>-induced cardiomyocyte apoptosis.

**Effects of G-CSF on cardiac function after myocardial infarction**  
Consistent with the *in vitro* data, G-CSF enhanced activation of Stat3 in the infarcted heart (Fig. 3a). Notably, the levels of G-CSFR were markedly increased after myocardial infarction in cardiomyocytes (Supplementary Fig. 4 online), which may enhance the effects of G-CSF on the infarcted heart. To elucidate the role of G-CSF-induced Stat3 activation in cardiac remodeling, we produced myocardial

infarction in transgenic mice which express dominant-negative Stat3 in cardiomyocytes under the control of the  $\alpha$ -myosin heavy chain promoter (dnStat3-Tg). Administration of G-CSF was started at the time of coronary artery ligation (day 0) until day 4 in transgenic mice; we termed this group Tg-G mice. A control group of dnStat3-Tg mice given myocardial infarction received saline (Tg-cont) instead of G-CSF. We also included two groups of wild-type mice given myocardial infarction treated with G-CSF (Wt-G) or saline (Wt-cont). At 2 weeks after myocardial infarction, we assessed the morphology by histological analysis and measured cardiac function by echocardiography and catheterization analysis. The infarct area was significantly smaller in the Wt-G group than the Wt-cont group (Fig. 3b). The Wt-G group also showed less left ventricular end-diastolic dimension (LVEDD) and better fractional shortening as assessed by echocardiography, and lower end-diastolic pressure (LVEDP) and better +dp/dt and -dp/dt as assessed by cardiac catheterization compared with Wt-cont (Fig. 3c). The beneficial effects of G-CSF on cardiac function were dose dependent and were significantly reduced by delayed start of the treatment (Fig. 3d,e and Supplementary Fig. 5 online). Moreover, its favorable effects on cardiac function became evident within 1 week after the treatment (Fig. 3f). Disruption of the Stat3 signaling pathway in cardiomyocytes abolished the protective effects of G-CSF. There was no significant difference in LVEDD, fractional shortening, LVEDP, +dp/dt and -dp/dt between Tg-G and Tg-cont (Fig. 3c). We obtained similar results from infarcted female hearts (Fig. 3g). These results suggest that G-CSF protects the heart after myocardial infarction at least in part by directly activating Stat3 in cardiomyocytes,

which is a gender-independent effect. We have previously shown that treatment with G-CSF significantly ( $P < 0.05$ ) decreased myocardial infarction-related mortality of wild-type mice<sup>2</sup>. In contrast, there were no significant differences in mortality between G-CSF-treated and saline-treated dnStat3-Tg mice (data not shown).

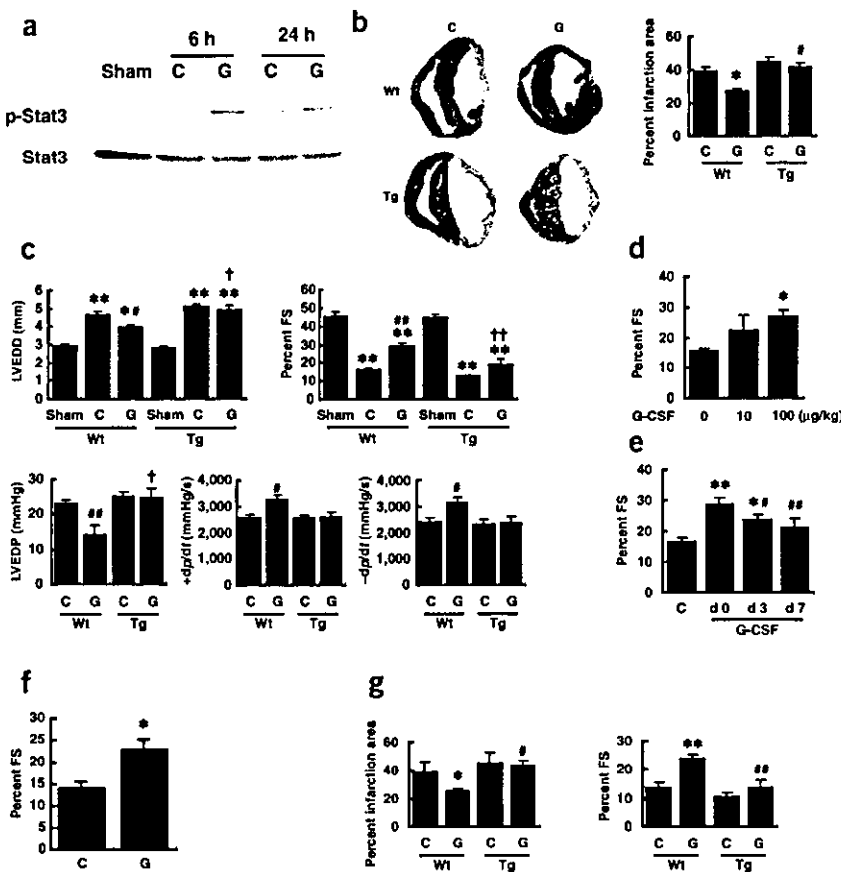


**Figure 3** Effects of G-CSF on cardiac function after myocardial infarction. (a) Stat3 activation in the infarcted hearts. We operated on wild-type mice to induce myocardial infarction and treated them with G-CSF (G) or saline (C). (b) Masson trichrome staining of wild-type (Wt) and dnStat3-Tg (Tg) hearts. \* $P < 0.001$  versus Wt-cont, # $P < 0.001$  versus Wt-G ( $n = 11-15$ ). (c) G-CSF treatment preserves cardiac function after myocardial infarction. \* $P < 0.01$ , \*\* $P < 0.001$  versus sham; # $P < 0.05$ , ## $P < 0.001$  versus Wt-cont; † $P < 0.01$ , †† $P < 0.001$  versus Wt-G ( $n = 10-15$  for echocardiography and  $n = 5$  for catheterization analysis). (d) Dose-dependent effects of G-CSF. FS, fractional shortening. \* $P < 0.01$  versus saline-treated mice (G-CSF = 0) ( $n = 12-14$ ). (e) Wild-type mice were operated to induce myocardial infarction and G-CSF treatment (100  $\mu\text{g}/\text{kg}/\text{d}$ ) was started from the indicated day for 5 d. \* $P < 0.05$ , \*\* $P < 0.001$  versus saline-treated mice (C); # $P < 0.05$ , ## $P < 0.01$  versus mice treated at day 0 (d 0) ( $n = 11-12$ ). (f) Effects of G-CSF on cardiac function at 1 week. \* $P < 0.05$  versus control ( $n = 3$ ). (g) Effects of G-CSF on cardiac function of female mice. \* $P < 0.05$ , \*\* $P < 0.001$  versus Wt-cont; # $P < 0.05$ , ## $P < 0.005$  versus Wt-G ( $n = 4-5$ ).

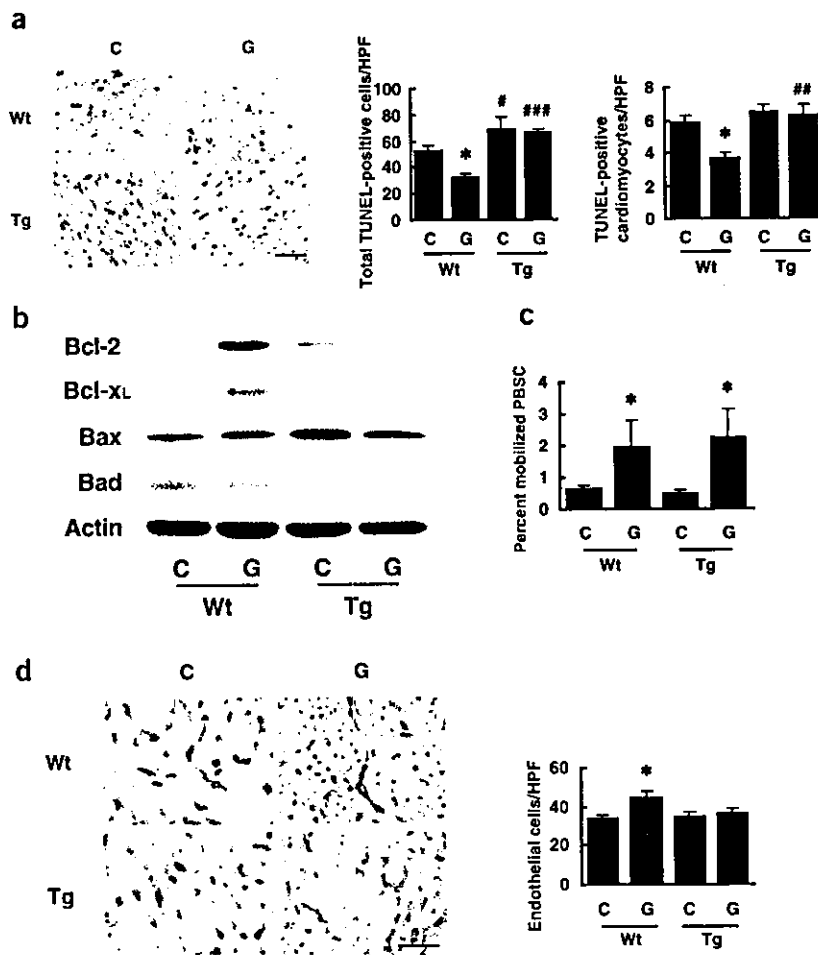


**Figure 4** Mechanisms of the protective effects of G-CSF. (a) TUNEL staining (brown nuclei) in the infarcted hearts. The graphs show quantitative analyses for total TUNEL-positive cells (left graph) and TUNEL-positive cardiomyocytes (right graph) in infarcted hearts. \* $P < 0.01$  versus Wt-cont; # $P < 0.05$ , ## $P < 0.005$ , ### $P < 0.001$  versus wild-type mice with the same treatment ( $n = 5-7$ ). Scale bar, 100  $\mu\text{m}$ . (b) Infarcted hearts treated with G-CSF (G) or saline (C) were analyzed for expression of Bcl-2, Bcl-xL, Bax and Bad by western blotting ( $n = 3$ ). (c) Mobilization of hematopoietic stem cells into peripheral blood (PBSC). \* $P < 0.05$  versus saline-treated mice ( $n = 4$ ). (d) Capillary endothelial cells were identified by immunohistochemical staining with anti-PECAM antibody in the border zone of the infarcted hearts. Scale bar, 100  $\mu\text{m}$ . The number of endothelial cells was counted and shown in the graph ( $n = 6-8$ ). \* $P < 0.05$ .

cently increased in the Wt-G group at 24 h after myocardial infarction compared with the Wt-cont group, whereas expression of the proapoptotic proteins Bax and Bad was not affected by the treatment (Fig. 4b). In contrast, expression levels of antiapoptotic proteins were not increased by G-CSF in the Tg-G group (Fig. 4b). Immunohistochemical analysis also showed increased expression of Bcl-2 in the infarcted heart of the Wt-G group but not of the Tg-G group (Supplementary Fig. 7 online).

To determine the effects of G-CSF on mobilization of stem cells, we counted the number of cells positive for both Sca-1 and c-kit in peripheral blood samples from mice treated with G-CSF or saline. The G-CSF treatment

#### Mechanisms of the protective effects of G-CSF

Our *in vitro* results suggest that the protective effects of G-CSF on cardiac remodeling after myocardial infarction can be attributed in part to reduction of cardiomyocyte apoptosis. To determine whether the Stat3 pathway in cardiomyocytes mediates the antiapoptotic effects of G-CSF on the ischemic myocardium, we carried out TUNEL labeling of left ventricular sections 24 h after myocardial infarction in wild-type mice and dnStat3-Tg mice. Although the number of TUNEL-positive cells was significantly less in the Wt-G group than the Wt-cont group, G-CSF treatment had no effect on cardiomyocyte apoptosis in dnStat3-Tg mice (Fig. 4a). The effects of G-CSF on apoptosis after myocardial infarction were also attenuated when mice were treated with AG490 (Supplementary Fig. 6 online). Myocardial infarction-related apoptosis was significantly increased in the Tg-cont group and AG490-treated wild-type mice compared with Wt-cont mice (Fig. 4a and Supplementary Fig. 6 online), suggesting that endogenous activation of Stat3 has a protective role in the infarcted heart, as reported previously<sup>25</sup>. It is noteworthy that G-CSF treatment inhibited apoptosis of noncardiomyocytes including endothelial cells and that this inhibition was abolished in dnStat3-Tg mice (Fig. 4a and data not shown). To investigate the underlying molecular mechanism of the antiapoptotic effects of G-CSF *in vivo*, we examined expression of the Bcl-2 protein family by western blot analysis. Consistent with our *in vitro* results, expression of antiapoptotic proteins such as Bcl-2 and Bcl-xL was signifi-

similarly increased the number of double-positive cells in wild-type mice and dnStat3-Tg mice (Fig. 4c). To examine the impact of G-CSF on cardiac homing of bone marrow cells, we transplanted bone marrow cells derived from GFP transgenic mice into wild-type and dnStat3-Tg mice, produced myocardial infarction and treated with G-CSF or saline. FACS analysis showed that G-CSF did not increase cardiac homing of bone marrow cells in wild-type and dnStat3-Tg mice (Supplementary Fig. 8 online). We have shown that cardiac stem cells, which are able to differentiate into cardiomyocytes, exist in Sca-1-positive populations in the adult myocardium<sup>26</sup>. But G-CSF treatment did not affect the number of Sca-1-positive cells in the infarcted hearts of wild-type or dnStat3-Tg mice (Supplementary Fig. 9 online). Thus, it is unlikely that G-CSF exerts its beneficial effects through expansion of cardiac stem cells. To determine the effects of G-CSF on proliferation of cardiomyocytes, we carried out immunostaining for Ki67, a marker for cell cycling, in conjunction with a labeling for troponin T. The number of Ki67-positive cardiomyocytes was increased in the infarcted hearts of wild-type mice and dnStat3-Tg mice compared with sham-operated mice (Supplementary Fig. 10 online). But G-CSF did not alter the number of Ki67-positive cardiomyocytes in wild-type or dnStat3-Tg mice, suggesting that G-CSF does not induce proliferation of cardiomyocytes (Supplementary Fig. 10 online). The number of Ki67-positive cardiomyocytes was less in infarcted hearts of dnStat3-Tg mice than in those of wild-type mice, suggesting that endogenous Stat3 activity is required



for myocardial regeneration after myocardial infarction and that activation of Stat3 by G-CSF is not sufficient for cardiomyocytes to enter the cell cycle in infarcted hearts of wild-type mice (Supplementary Fig. 10 online). In contrast, G-CSF treatment significantly increased the number of endothelial cells in the border zone of the infarcted hearts (Fig. 4d). This increase was attenuated in dnStat3-Tg mice, indicating that the increased vascularity is mediated by Stat3 activity in cardiomyocytes and may partially account for the beneficial effects of G-CSF on the infarcted hearts. Taken together with the result that G-CSF-induced inhibition of noncardiomyocyte apoptosis was also mediated by the Stat3 signaling pathway in cardiomyocytes (Fig. 4a), these findings imply that communication between cardiomyocytes and noncardiomyocytes regulates each others' survival.

To further test whether G-CSF acts directly on the heart, we examined the effects of G-CSF treatment on cardiac function after ischemia-reperfusion injury in a Langendorff perfusion model. The isolated hearts underwent 30 min total ischemia followed by 120 min reperfusion with the perfusate containing G-CSF (300 ng/ml) or vehicle, and left ventricular developed pressure (LVDP, measured as the difference between systolic and diastolic pressures of the left ventricle) and LVEDP were measured. There were no significant differences in basal hemodynamic parameters including heart rate, left ventricular pressure, LVEDP and positive and negative  $dp/dt$ , between the control group and G-CSF group (Table 1). After reperfusion, however, G-CSF-treated hearts started to beat earlier than those of the control group (Fig. 5a). At 120 min after reperfusion, contractile function (LVDP) of G-CSF-treated hearts was significantly better than that of control hearts (Fig. 5a). Likewise, diastolic function (LVEDP) of G-CSF-treated hearts was better than that of control hearts (Fig. 5a). After ischemia-reperfusion, there was more viable myocardium (red lesion) in G-CSF-treated hearts than control

**Table 1** Basal hemodynamic parameters

	Control (n = 7)	G-CSF (n = 7)
HR (b.p.m.)	326 ± 34	334 ± 24
LVP (mmHg)	121.8 ± 24	117.3 ± 32
LVEDP (mmHg)	4.3 ± 1.3	4.5 ± 1.6
+dp/dt (mmHg/s)	7,554 ± 643	7,657 ± 377
-dp/dt (mmHg/s)	6,504 ± 638	6,670 ± 602

HR, heart rate; b.p.m., beats per minute; LVP, left ventricular pressure; LVEDP, left ventricular end-diastolic pressure; +dp/dt and -dp/dt, positive and negative first derivatives for maximal rates of left ventricular pressure development.

hearts (Fig. 5b). The size of the infarct (white lesion) was significantly smaller in G-CSF-treated hearts than in control hearts (Fig. 5b).

## DISCUSSION

In the present study, G-CSFR was found to be expressed on cardiomyocytes and cardiac fibroblasts, and G-CSF activated Jak2 and the downstream signaling molecule Stat3 in cultured cardiomyocytes. Treatment with G-CSF protected cultured cardiomyocytes from apoptotic cell death possibly through upregulation of Bcl-2 and Bcl-xL expression, suggesting that G-CSF has direct protective effects on cardiomyocytes through G-CSFR and the Jak-Stat pathway. This idea is further supported by the *in vivo* experiments. G-CSF enhanced Stat3 activity and increased expression of Bcl-2 and Bcl-xL in the infarcted heart where G-CSFR was markedly upregulated, thereby preventing cardiomyocyte apoptosis and cardiac dysfunction. These effects of G-CSF were abolished when Stat3 activation was disrupted in cardiomyocytes, suggesting that a direct action of G-CSF on cardiomyocytes has a crucial role in preventing left ventricular remodeling after myocardial infarction. Because noncardiomyocytes also expressed G-CSFR, the possibility exists that activation of G-CSF receptors on these cells modulates the beneficial effects of G-CSF on infarcted hearts.

The mobilization of bone marrow stem cells (BMSC) to the myocardium has been considered to be the main mechanism by which G-CSF ameliorates cardiac remodeling after myocardial infarction<sup>1,6-8</sup>. In this study, we showed that G-CSF reduces apoptotic cell death and effectively protects the infarcted heart, which is dependent on its direct action on cardiomyocytes through the Stat3 pathway. This antiapoptotic mechanism seems to be more important than induction of BMSC mobilization, because disruption of

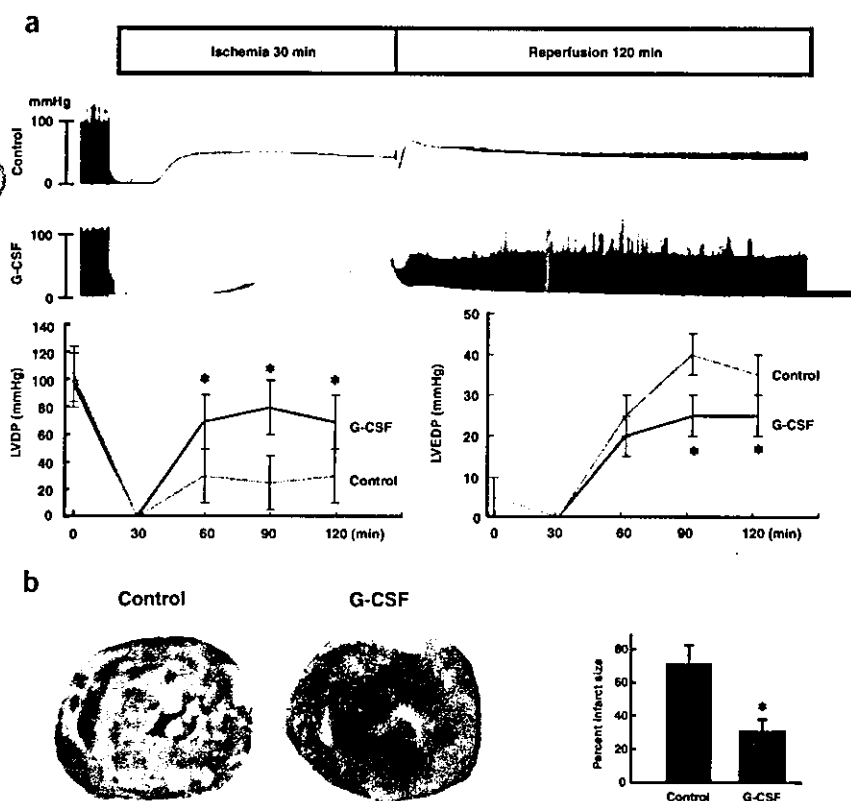


**Figure 5** Direct effects of G-CSF on cardiac function after ischemia-reperfusion injury. (a) Representative left ventricular pressure records of control and G-CSF-treated hearts are shown (upper panel). The graphs show changes in LVDP (left) and LVEDP (right) during ischemia-reperfusion. \* $P < 0.05$  versus control hearts ( $n = 7$ ). (b) The photographs show representative TTC staining of control hearts (Control) and G-CSF-treated hearts (G-CSF) after ischemia-reperfusion. The graph indicates myocardial infarct sizes for control hearts (Control) and G-CSF-treated hearts (G-CSF). Infarct sizes were calculated as described in Supplementary Methods online. \* $P < 0.05$  versus control hearts ( $n = 7$ ).

## ARTICLES

this pathway by expressing dnStat3 in cardiomyocytes almost abolished the protective effects of G-CSF on cardiac remodeling after myocardial infarction. In addition, there was no difference in the effects of G-CSF on mobilization and cardiac homing of bone marrow cells, expansion of cardiac stem cells, and proliferation of cardiomyocytes between wild-type and dnStat3-Tg mice. The beneficial effects of G-CSF and stem cell factor on the infarcted heart has been described, but no evidence indicating that G-CSF induced cardiac homing of bone marrow cells in the infarcted heart has been shown<sup>1</sup>. In this study, we found favorable effects of G-CSF on the infarcted heart as early as 1 week after the treatment even though cardiac homing of bone marrow cells was not increased. Thus, we conclude that increased cardiac homing of bone marrow cells cannot account for improved function of the infarcted heart after G-CSF treatment.

The JAK-STAT pathway has been shown to induce various angiogenic factors besides antiapoptotic proteins<sup>20,21</sup>. The number of endothelial cells in the border zone was increased by G-CSF through Stat3 activation in cardiomyocytes. Consistent with this, we noted that G-CSF induces cardiac expression of angiogenic factors *in vitro* and *in vivo*, which appears to be mediated by cardiac Stat3 activation (M.H., Y.Q., H.T., T.M. & I.K., unpublished data). Moreover, we observed that the majority of apoptotic cells in the infarcted hearts was endothelial cells and that endothelial apoptosis was significantly inhibited by G-CSF treatment in wild-type mice but not in dnStat3-Tg mice (Fig. 4a and M.H., T.M. & I.K., unpublished data). Thus, activation of this pathway in cardiomyocytes by G-CSF may also promote angiogenesis and protect against endothelial apoptosis by producing angiogenic factors, resulting in the further prevention of cell death of cardiomyocytes and cardiac remodeling after myocardial infarction. The results in this study provide new mechanistic insights of the G-CSF therapy on infarcted hearts.

### METHODS

For further details, please see **Supplementary Methods** online.

**Cell culture.** Cardiomyocytes prepared from ventricles of 1-d-old Wistar rats<sup>27</sup> were plated onto 60-mm plastic culture dishes at a concentration of  $1 \times 10^5$  cells/cm<sup>2</sup> and cultured in Dulbecco modified Eagle medium (DMEM) supplemented with 10% fetal bovine serum (FBS) at 37 °C in a mixture of 95% air and 5% CO<sub>2</sub>. The culture medium was changed to serum-free DMEM 24 h before stimulation. Generation and infection of recombinant adenovirus were performed as described<sup>28</sup>.

**Percoll enrichment of adult mouse cardiomyocytes and noncardiomyocytes.** Adult mouse cardiomyocytes were prepared from 10-week-old C57BL/6 male mice according to the Alliance for Cellular Signaling protocol. We also prepared cardiomyocytes and noncardiomyocytes from myocardial infarction-operated or sham-operated C57BL/6 male mice. After digestion, cells were dissociated, resuspended in differentiation medium and loaded onto a discontinuous Percoll gradient. Cardiomyocytes or noncardiomyocytes were separately collected as described previously<sup>29</sup> and subsequently washed with  $1 \times$  phosphate-buffered saline for RT-PCR.

**RNA extraction and RT-PCR analysis.** Total RNA from adult mice cardiomyocytes was isolated by the guanidinium thiocyanate-phenol chloroform method. A total of 4 µg RNA was transcribed with MMLV reverse transcriptase and random hexamers. The cDNA was amplified using a mouse *Csf3r* exon 15 forward primer (5'-GTACTCTGTCCACTACTGT-3') and an exon 17 reverse primer (5'-CAAGATACAAGGACCCCAA-3'). We performed PCR under the following conditions: an initial denaturation at 94 °C for 2 min followed by a cycle of denaturation at 94 °C for 1 min, annealing at 58 °C for 1 min and extension at 72 °C for 1 min. We subjected samples to 40 cycles followed by a final extension at 72 °C for 3 min. The products were analyzed on a 1.5% ethidium bromide stained agarose gel.

**Immunocytochemistry.** Cardiomyocytes or noncardiomyocytes of neonatal rats cultured on glass cover slips were incubated with or without the antibody to G-CSFR (Santa Cruz Biotechnology) for 1 h, followed by incubation with Cy3-labeled secondary antibodies. After washing, we double-stained the cells with fluorescent phalloidin (Molecular Probes) for 1 h at room temperature.

**Western blots.** Western blot analysis was performed as described<sup>5</sup>. We probed the membranes with antibodies to phospho-Jak2, phospho-Stat3 (Cell Signaling), phospho-Jak1, phospho-Tyk2, phospho-Stat1, phospho-Stat5, anti-Jak1, Jak2, Tyk2, Stat1, Stat3, Stat5, Bcl-2, Bax, G-CSFR (Santa Cruz Biotechnology), Bcl-xL, Bad (Transduction Laboratories) or actin (Sigma-Aldrich). We used the ECL system (Amersham Biosciences Corp) for detection.

**Animals and surgical procedures.** Generation and genotyping of dnStat3-Tg mice have been previously described<sup>28</sup>. All mice used in this study were 8–10-week-old males, unless indicated. All experimental procedures were performed according to the guidelines established by Chiba University for experiments in animals and all protocols were approved by our institutional review board. We anesthetized mice by intraperitoneally injecting a mixture of 100 mg/kg ketamine and 5 mg/kg xylazine. Myocardial infarction was produced by ligation of the left anterior descending artery. We operated on dnStat3-Tg mice to induce myocardial infarction and randomly divided them into two groups, the G-CSF-treated group (10–100 µg/kg/d subcutaneously for 5 d consecutively, Kyowa Hakko Kogyo Co.) and the saline-treated group. We operated on nontransgenic mice as control groups using the same procedures and divided them into a G-CSF-treated group and a saline-treated group. Some mice were randomly chosen to be analyzed for initial area at risk by injection of Evans blue dye after producing myocardial infarction. There was no difference in initial area sizes at risk between saline-treated control and G-CSF-treated mice ( $n = 5$ ; **Supplementary Fig. 11** online). We also determined initial infarct size by triphenyltetrazolium chloride staining on day 3. There was no significant difference in initial infarct size between saline-treated control and G-CSF-treated mice ( $n = 5$ ; **Supplementary Fig. 12** online).

**Echocardiography and catheterization.** Transthoracic echocardiography was performed with an Agilent Sonos 4500 (Agilent Technology Co.) provided with an 11-MHz imaging transducer. For catheterization analysis, the right carotid artery was cannulated under anesthesia by the micro pressure transducers with an outer diameter of 0.42 mm (Samba 3000; Samba Sensors AB), which was then advanced into the left ventricle. Pressure signals were recorded using a MacLab 3.6/s data acquisition system (AD Instruments) with a sampling rate of 2,000 Hz. Mice were anesthetized as described above, and heart rate was kept at approximately 270–300 beats per minute to minimize data deviation when we measured cardiac function.

**Histology.** Hearts fixed in 10% formalin were embedded in paraffin, sectioned at 4 µm thickness, and stained with Masson trichrome. The extent of fibrosis was measured in three sections from each heart and the value was expressed as the ratio of Masson trichrome stained area to total left ventricular free wall. For apoptosis analysis, infarcted hearts were frozen in cryomolds, sectioned, and TUNEL labeling was performed according to the manufacturer's protocol (*In Situ* Apoptosis Detection kit; Takara) in combination with immunostainings for appropriate cell markers. Digital photographs were taken at magnification  $\times 400$ , and 25 random high-power fields (HPF) from each heart sample were chosen and quantified in a blinded manner. We examined vascularization by measuring the number of capillary endothelial cells in light-microscopic sections taken from the border zone of the hearts 2 weeks after myocardial infarction. Capillary endothelial cells were identified by immunohistochemical staining with antibody to platelet endothelial cell adhesion molecule (PECAM; Pharmingen). Ten random microscopic fields in the border zone were examined and the number of endothelial cells was expressed as the number of PECAM-positive cells/HPF (magnification,  $\times 400$ ).

**Statistical analysis.** Data are shown as mean  $\pm$  s.e.m. Multiple group comparison was performed by one-way analysis of variance (ANOVA) followed by the Bonferroni procedure for comparison of means. Comparison between two groups were analyzed by the two-tailed Student's *t*-test or two-way ANOVA. Values of  $P < 0.05$  were considered statistically significant.



URL. Alliance for Cellular Signaling Procedure Protocols  
<http://www.signaling-gateway.org/data/cgi-bin/Protocols.cgi?cat=0>

Note: Supplementary information is available on the Nature Medicine website.

#### ACKNOWLEDGMENTS

The authors thank J. Robbins (Children's Hospital Research Foundation, Cincinnati, Ohio) for a fragment of the  $\alpha$ MHC gene promoter, M. Tamagawa for the analysis of Langendorff-perfused model, Kirin Brewery Co., Ltd. for their kind gift of G-CSF, and M. Watanabe and E. Fujita for their technical assistance. This work was supported by a Grant-in-Aid for Scientific Research, Developmental Scientific Research, and Scientific Research on Priority Areas from the Ministry of Education, Science, Sports, and Culture and by the Program for Promotion of Fundamental Studies in Health Sciences of the Organization for Drug ADR Relief, R&D Promotion and Product Review of Japan (to I.K.) and Japan Research Foundation for Clinical Pharmacology (to T.M.).

#### COMPETING INTERESTS STATEMENTS

The authors declare that they have no competing financial interests.

Received 8 September 2004; accepted 19 January 2005

Published online at <http://www.nature.com/naturemedicine/>

- Orlic, D. *et al.* Mobilized bone marrow cells repair the infarcted heart, improving function and survival. *Proc. Natl. Acad. Sci. USA* **98**, 10344–10349 (2001).
- Ohtsuka, M. *et al.* Cytokine therapy prevents left ventricular remodeling and dysfunction after myocardial infarction through neovascularization. *FASEB J.* **18**, 851–853 (2004).
- Moon, C. *et al.* Erythropoietin reduces myocardial infarction and left ventricular functional decline after coronary artery ligation in rats. *Proc. Natl. Acad. Sci. USA* **100**, 11612–11617 (2003).
- Parsa, C.J. *et al.* A novel protective effect of erythropoietin in the infarcted heart. *J. Clin. Invest.* **112**, 999–1007 (2003).
- Zou, Y. *et al.* Leukemia inhibitory factor enhances survival of cardiomyocytes and induces regeneration of myocardium after myocardial infarction. *Circulation* **108**, 748–753 (2003).
- Minatoguchi, S. *et al.* Acceleration of the healing process and myocardial regeneration may be important as a mechanism of improvement of cardiac function and remodeling by postinfarction granulocyte colony-stimulating factor treatment. *Circulation* **109**, 2572–2580 (2004).
- Adachi, Y. *et al.* G-CSF treatment increases side population cell infiltration after myocardial infarction in mice. *J. Mol. Cell. Cardiol.* **36**, 707–710 (2004).
- Kawada, H. *et al.* Nonhematopoietic mesenchymal stem cells can be mobilized and differentiate into cardiomyocytes after myocardial infarction. *Blood* **104**, 3581–3587 (2004).
- Avalos, B.R. Molecular analysis of the granulocyte colony-stimulating factor receptor. *Blood* **88**, 761–777 (1996).
- Demetri, G.D. & Griffin, J.D. Granulocyte colony-stimulating factor and its receptor. *Blood* **78**, 2791–808 (1991).
- Berliner, N. *et al.* Granulocyte colony-stimulating factor induction of normal human bone marrow progenitors results in neutrophil-specific gene expression. *Blood* **85**, 799–803 (1995).
- Orlic, D. *et al.* Bone marrow cells regenerate infarcted myocardium. *Nature* **410**, 701–705 (2001).
- Asahara, T. *et al.* Bone marrow origin of endothelial progenitor cells responsible for postnatal vasculogenesis in physiological and pathological neovascularization. *Circ. Res.* **85**, 221–228 (1999).
- Kocher, A.A. *et al.* Neovascularization of ischemic myocardium by human bone-marrow-derived angioblasts prevents cardiomyocyte apoptosis, reduces remodeling and improves cardiac function. *Nat. Med.* **7**, 430–436 (2001).
- Jackson, K.A. *et al.* Regeneration of ischemic cardiac muscle and vascular endothelium by adult stem cells. *J. Clin. Invest.* **107**, 1395–1402 (2001).
- Balsam, L.B. *et al.* Haematopoietic stem cells adopt mature haematopoietic fates in ischaemic myocardium. *Nature* **428**, 668–673 (2004).
- Murry, C.E. *et al.* Haematopoietic stem cells do not transdifferentiate into cardiac myocytes in myocardial infarcts. *Nature* **428**, 664–668 (2004).
- Norol, F. *et al.* Influence of mobilized stem cells on myocardial infarct repair in a nonhuman primate model. *Blood* **102**, 4361–4368 (2003).
- Aarts, L.H., Roovers, O., Ward, A.C. & Touw, I.P. Receptor activation and 2 distinct COOH-terminal motifs control G-CSF receptor distribution and internalization kinetics. *Blood* **103**, 571–579 (2004).
- Benekli, M., Baer, M.R., Baumann, H. & Wetzler, M. Signal transducer and activator of transcription proteins in leukemias. *Blood* **101**, 2940–2954 (2003).
- Smithgall, T.E. *et al.* Control of myeloid differentiation and survival by Stats. *Oncogene* **19**, 2612–2618 (2000).
- Dumont, E.A. *et al.* Cardiomyocyte death induced by myocardial ischemia and reperfusion: measurement with recombinant human annexin-V in a mouse model. *Circulation* **102**, 1564–1568 (2000).
- van Heerde, W.L. *et al.* Markers of apoptosis in cardiovascular tissues: focus on Annexin V. *Cardiovasc. Res.* **45**, 549–559 (2000).
- Bromberg, J. Stat proteins and oncogenesis. *J. Clin. Invest.* **109**, 1139–1142 (2002).
- El-Adawi, H. *et al.* The functional role of the JAK-STAT pathway in post-infarction remodeling. *Cardiovasc. Res.* **57**, 129–138 (2003).
- Matsuura, K. *et al.* Adult cardiac Sca-1-positive cells differentiate into beating cardiomyocytes. *J. Biol. Chem.* **279**, 11384–11391 (2004).
- Zou, Y. *et al.* Both Gs and Gi proteins are critically involved in isoproterenol-induced cardiomyocyte hypertrophy. *J. Biol. Chem.* **274**, 9760–9770 (1999).
- Funamoto, M. *et al.* Signal transducer and activator of transcription 3 is required for glycoprotein 130-mediated induction of vascular endothelial growth factor in cardiac myocytes. *J. Biol. Chem.* **275**, 10561–10566 (2000).
- Ikeda, K. *et al.* The effects of sarpgrelate on cardiomyocyte hypertrophy. *Life Sci.* **67**, 2991–2996 (2000).





## Reciprocal regulation of permeability through a cultured keratinocyte sheet by IFN- $\gamma$ and IL-4

Junichi Kobayashi<sup>a,b,\*</sup>, Tetsuichiro Inai<sup>a</sup>, Keisuke Morita<sup>b</sup>, Yoichi Moroi<sup>b</sup>, Kazunori Urabe<sup>b</sup>, Yosaburo Shibata<sup>a</sup>, Masutaka Furue<sup>b</sup>

<sup>a</sup>Department of Developmental Molecular Anatomy, Graduate School of Medical Sciences, Kyushu University, Fukuoka 812-8582, Japan

<sup>b</sup>Department of Dermatology, Graduate School of Medical Sciences, Kyushu University, Fukuoka 812-8582, Japan

Received 24 November 2003; received in revised form 19 May 2004; accepted 2 August 2004

### Abstract

The T cell cytokines profoundly modify the phenotypic and functional characteristics of keratinocytes. Until now, no study has focused on the effect of Th1 and Th2 cytokines on keratinocyte permeability. Using a two-layer well culturing system, permeability was assessed through cultured keratinocyte sheet in the presence or absence of various concentrations of IFN- $\gamma$  and IL-4. Transepithelial electrical resistance (TER) and the flux of 40 kDa FITC-dextran were measured across the cultured keratinocyte sheet. IFN- $\gamma$  significantly increased the TER in a dose- and time-dependent manner, suggesting that IFN- $\gamma$  profoundly inhibited the permeability of ions through the keratinocyte sheet. In contrast, IL-4 did not affect the TER. When compared to medium control, the flux of FITC-dextran of the IFN- $\gamma$  group was significantly decreased in a dose-dependent fashion. In sharp contrast, the flux of FITC-dextran was significantly and dose-dependently increased in the presence of IL-4. A significant increase in TER and a significant decrease in the flux of dextran suggested that IFN- $\gamma$  clearly reduced the permeability of both ions and high molecular weight material through the keratinocyte sheet. Although IL-4 did not affect the permeability of the ions, it significantly enhanced the permeability of high molecular weight material. A flow cytometric assay revealed that the expression of desmoglein-3 was suppressed by IL-4, but was enhanced by IFN- $\gamma$ . The reciprocal regulation of permeability of the cultured keratinocyte sheet by IFN- $\gamma$  and IL-4 may be partly related to the modification of intercellular adhesion molecules.

© 2004 Elsevier Ltd. All rights reserved.

**Keywords:** Keratinocyte; Permeability; IFN- $\gamma$ ; IL-4

### 1. Introduction

Epidermis, a squamous epithelium of the skin, serves as the outermost barrier of the body, separating it from the surrounding environment and preventing the loss of body fluids and proteins. Very frequently, immunological and inflammatory processes result in skin damage in

eczematous disorders such as contact dermatitis and atopic dermatitis [1,2]. Eczema is an orchestrated cellular response conducted by various immunocompetent cells, including Th1 and the Th2 cells, that produce large amounts of cytokines such as IFN- $\gamma$  and IL-4, respectively [3,4]. One of the characteristic manifestations of eczema is serous papules with spongiosis and oozing, which may result from an increased permeability of body fluids into the epidermal compartment.

Previous studies have shown that T cell cytokines profoundly modify the phenotypic and functional characteristics of keratinocytes [5,6]. However, there have been no reports investigating the effect of Th1 and

\* Corresponding author. Division of Dermatology, Nippon Steel Yawata Memorial Hospital, 1-1-1, Harunomachi, Yahatahigashi-ku, Kitakyushu J-805-8508, Japan. Tel.: +81 93 672 3176; fax: +81 93 671 9605.

E-mail address: jkobayashi@jcom.home.ne.jp (J. Kobayashi).